Chemistry–A European Journal

Supporting Information

CryoEM Structure with ATP Synthase Enables Late-Stage Diversification of Cruentaren A

Xiaozheng Dou, Hui Guo, Terin D'Amico, Leah Abdallah, Chitra Subramanian, Bhargav A. Patel, Mark Cohen, John L. Rubinstein, and Brian S. J. Blagg*

Table of Contents:

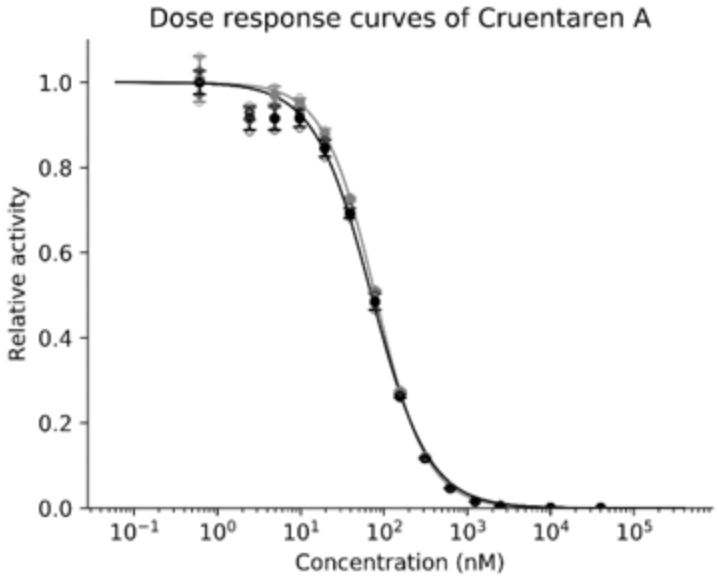

Figure S1. Cruentaren A inhibits ATP hydrolysis by purified ATP synthase. The dose response curves were measured using a pyruvate kinase/lactose dehydrogenase coupled assay. The mean values (filled symbols) from two independently purified protein batches (black and gray circles) are shown, with n = 3 separate assays for each protein batch at each drug concentration. Data are presented as mean values ± s.d. Full activity is defined at 0 nM cruentaren A.

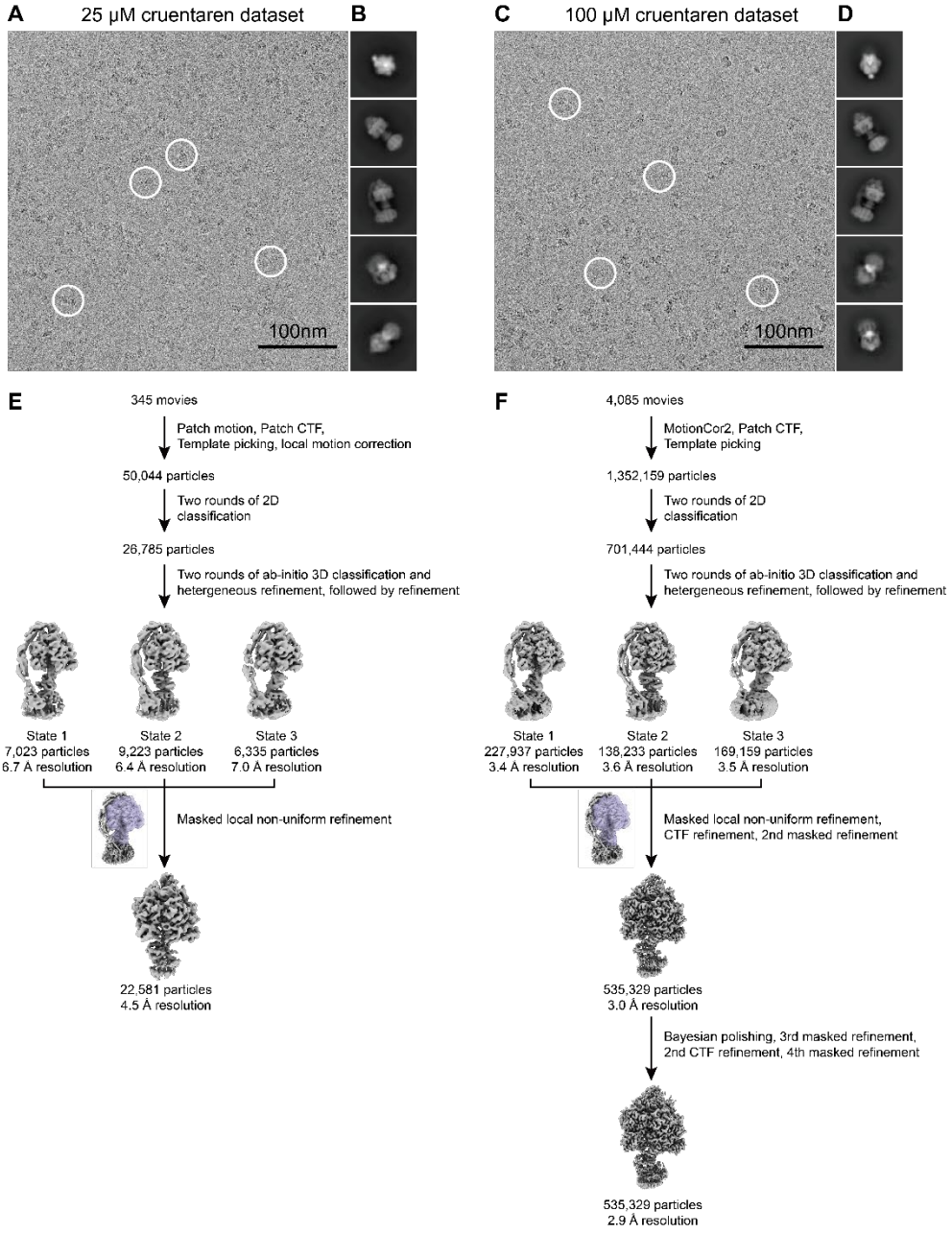

Figure S2. Workflow for cryo-EM image analysis. Example micrographs (**A, C**), 2D class average images (**B, D**), and workflow for obtaining maps of the F_1 regions (**E, F**) for 25 μM and 100 μM cruentaren-bound ATP synthases, respectively.

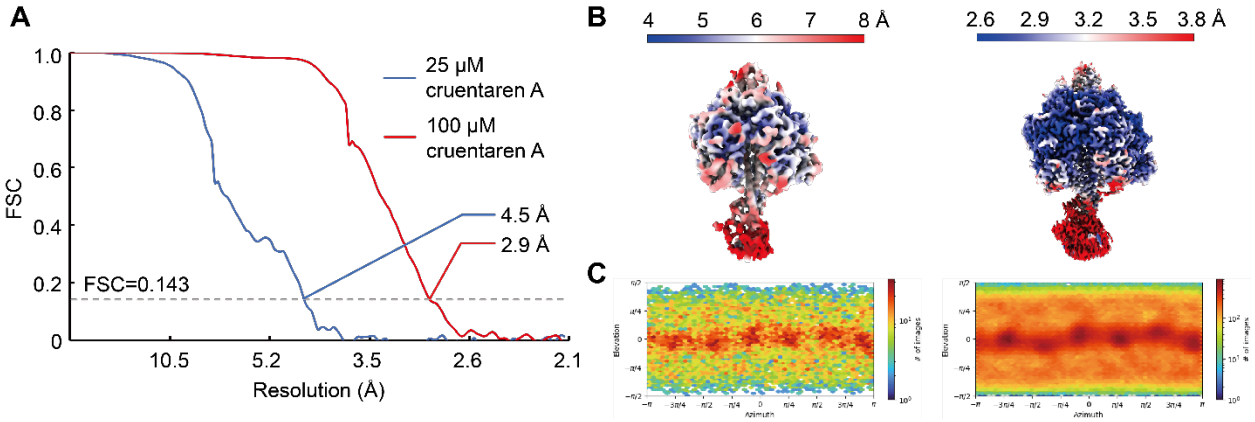

Figure S3. CryoEM map validation. Fourier shell correlation curves after gold-standard refinement corrected for masking(**A**), local resolution maps (**B**), and orientation distribution plots (**C**) are shown for the maps of the F_1 regions from the 25 µM and 100 µM cruentaren-bound datasets.

Table S1. Cryo-EM data collection, refinement, and validation statistics.

	yF_1F_O 25 μM cruentaren A (EMDB-28819)	yF_1F_O 100 μM cruentaren A (EMDB-28818) (PDB 8F2K)
Data collection and processing		
Magnification	75,000	75,000
Voltage (kV)	300	300
Electron exposure (e–/Å^2)	37	42
Defocus range (μm)	0.9-3.3	0.6-2.9
Movie pixel size (Å)	1.04622	1.04622
Symmetry imposed	C1	C1
Initial particle images (no.)	50,044	1,352,159
Final particle images (no.)	22,581	535,329
Map resolution (Å)	4.5	2.9
FSC threshold	0.143	0.143
Refinement		
Initial model used (PDB code)		7MD2
Model resolution (Å)		3.0
FSC threshold		0.5
Map sharpening *B* factor (Å^2)		-109.2
Model composition		
Non-hydrogen atoms		22402
Protein residues		2962
Ligands		12
B factors (Å^2)		
Protein		72.56
Ligand		70.13
R.m.s. deviations		
Bond lengths (Å)		0.003
Bond angles (°)		0.786
Validation		
MolProbity score		1.07
Clashscore		2.80
Poor rotamers (%)		0.74
Ramachandran plot		
Favored (%)		98.40
Allowed (%)		1.56
Disallowed (%)		0.03

ATP synthase purification
Preparation of yeast ATP synthase solubilized by dodecyl-β-D-maltoside (DDM, Anatrace) followed the same protocol as described previously[1,2]. Purified ATP synthase was concentrated to ~10 or 20 mg/ml (~16.7 or 33.3 μM) and stored at −80 °C until use.

Enzyme-coupled ATPase assay for ATP synthase
ATPase assays were performed as described previously[3,4] in 96-well plates with 160 μl buffer (50 mM Tris–HCl pH 7.4, 150 mM NaCl, 10% (v/v) glycerol, 5 mM $MgCl_2$, 0.2 mM NADH, 2 mM ATP, 1 mM phosphoenol pyruvate, 3.2 units pyruvate kinase, 8 units lactate dehydrogenase, 0.05% (w/v) dodecyl-β-D-maltoside, dimethylsulfoxide (v/v) 2%, 2 nM ATP synthase). NADH concentration was monitored at 24 °C with a Synergy Neo2 Multi-Mode Assay Microplate Reader (BioTek) measuring absorbance at 340 nm. Inhibition with cruentaren A was determined by adding different concentrations of the inhibitor to the assay mixture. Assays were performed in triplicate with two independently purified batches of yeast ATP synthase.

CryoEM grid preparation
Purified yeast ATP synthase (20 mM Tris-HCl pH 7.4, 10% [v/v] glycerol, 0.05% [w/w] DDM, 100 mM NaCl, 5 mM $MgCl_2$) at 10 and 20mg/ml was incubated with 25 μM and 100 μM cruentaren A for 1 hour at 4 °C, respectively. Glycerol in the sample was removed with Zeba Spin Desalting Column (ThermoFisher Scientific) equilibrated with buffer containing the same concentrations of cruentaren A immediately before freezing. Cruentaren-bound, glycerol-free ATP synthase was then applied to homemade[5] holey-gold grids that had been glow discharged in air for 2 min. Grids were blotted with EM GP2 (Leica) for 1 s with ~95% humidity at 4 °C before being plunge frozen in a liquid ethane/propane mixture[6].

CryoEM data collection
CryoEM movies of yeast ATP synthase bound to 25 μM or 100 μM cruentaren were collected with a Titan Krios G3 electron microscope operated at 300 kV and equipped with a prototype Falcon 4 camera (ThermoFisher Scientific). Automatic data collection was performed with EPU (ThermoFisher Scientific). Both 25 μM and 100 μM cruentaren datasets were collected at a nominal magnification of ×75,000, corresponding to a calibrated pixel size of 1.046 Å. For the 25 μM cruentaren dataset, 345 movies each containing 29 fractions were collected with a total exposure and a camera exposure rate of ~37 $e^- Å^{-2}$ and 5.0 $e^- pixel^{-1} s^{-1}$, respectively. The 100 μM cruentaren dataset consists of 5,814 movies each containing 29 fractions. The total exposure and the camera exposure rate of the movies are ~42 $e^- Å^{-2}$ and 5.0 $e^- pixel^{-1} s^{-1}$, respectively.

Image analysis
Image analysis was performed with cryoSPARC v2[7] except where noted. For the 25 μM cruentaren dataset containing 345 movies, movie frames were aligned with patch motion correction[8] and contrast transfer function (CTF) parameters were estimated with patch CTF estimation. For the 100 μM cruentaren dataset that contains 5,814 movies, movie frames were aligned with MotionCor2 using a 7 × 7 grid and CTF parameters were estimated with patch CTF estimation. Movies with undesirable motion or CTF fit were removed, leaving 4,084 movies for further processing. Two templates showing a sideview and an oblique view of ATP synthase were generated by two-dimensional (2D) classification of ~500 manually selected particle images with

a box size of 320 × 320. Template picking selected 50,044 particles for the 25 μM cruentaren dataset and 1,352,159 particles for the 100 μM cruentaren dataset. For the 25 μM cruentaren dataset, beam-induced motion was re-estimated by local motion correction. Cleaning by 2D classification yielded 26,785 and 701,444 particles for the 25 μM and 100 μM cruentaren datasets, respectively. Ab initio three-dimensional (3D) classification and heterogeneous refinement further cleaned particle images and identified three conformations corresponding to the three rotational states of ATP synthase. Non-uniform refinement[9] was performed for each of the three classes, which was followed by a masked local refinement with particles from all three classes around the F_1 region of ATP synthase. This local refinement yielded a 4.5 Å resolution map from 22,581 particle images for the 25 μM cruentaren dataset, and a 3.0 Å resolution structure from 535,329 particle images for the 100 μM cruentaren dataset after defocus refinement. To further improve the map from the 100 μM cruentaren dataset, image parameters from cryoSPARC were converted to Relion[10] star file format with the pyem package (https://doi.org/10.5281/zenodo.3576630) and individual particle motion was re-estimated with Bayesian polishing[11]. Particle images were then imported back to cryoSPARC and another cycle of local refinement, CTF refinement, and second local refinement around the F_1 region was performed, yielding a final map of 2.9 Å resolution.

Atomic model building

To model the F_1 region of the cruentaren-bound structure, individual subunits of the F_1 region of a yeast ATP synthase crystal structure (2XOK) were fit rigidly into the ammocidin map with UCSF Chimera. The model was then manually adjusted in Coot and ISOLDE before being refined in Phenix.

Antiproliferative assay

The proliferation of three cancer cell lines (MCF7, K562, and A549) after treatment with varying concentrations of Crentaren A and its analogues was measured by the CellTiter Glo assay. About 750- 1000 cells per well were plated in clear bottom 96 well plates, and the cells were allowed to attach for 24h. Post plating, the cells were treated with serial dilutions of drugs starting from 4 mM. The cells were treated with the CellTiter Glow reagent (Promega), both before the addition of drugs and after 72h post-treatment. ATP present that is a direct measure of proliferation was quantified by measuring luminescence in a Synergy BioTEK plate reader. Growth inhibition was calculated by using the NCI 60 screening assay protocol. The GI50 values were calculated by GraphPad Prism software using solvent DMSO treated cells as control. The GI50 values represent the average of the two independent experiments done in triplicate.

References

(1) Guo, H.; Rubinstein, J. L. Structure of ATP Synthase under Strain during Catalysis. *Nat Commun* **2022**, *13* (1), 2232. https://doi.org/10.1038/s41467-022-29893-2.

(2) Reisman, B. J.; Guo, H.; Ramsey, H. E.; Wright, M. T.; Reinfeld, B. I.; Ferrell, P. B.; Sulikowski, G. A.; Rathmell, W. K.; Savona, M. R.; Plate, L.; Rubinstein, J. L.; Bachmann, B. O. Apoptolidin Family Glycomacrolides Target Leukemia through Inhibition of ATP Synthase. *Nat Chem Biol* **2022**, *18* (4), 360–367. https://doi.org/10.1038/s41589-021-00900-9.

(3) KORNBERG, A.; PRICER, W. E. Enzymatic Phosphorylation of Adenosine and 2,6-Diaminopurine Riboside. *The Journal of biological chemistry* **1951**, *193* (2), 481–495. https://doi.org/10.1016/s0021-9258(18)50904-2.

(4) Guo, H.; Courbon, G. M.; Bueler, S. A.; Mai, J.; Liu, J.; Rubinstein, J. L. Structure of Mycobacterial ATP Synthase with the TB Drug Bedaquiline. *Nature* **2021**, *589* (Jan 2020), 143–147. https://doi.org/10.1038/s41586-020-3004-3.

(5) Marr, C. R.; Benlekbir, S.; Rubinstein, J. L. Fabrication of Carbon Films with ~500nm Holes for Cryo-EM with a Direct Detector Device. *Journal of Structural Biology* **2014**, *185* (1), 42–47. https://doi.org/10.1016/j.jsb.2013.11.002.

(6) Tivol, W. F.; Briegel, A.; Jensen, G. J. An Improved Cryogen for Plunge Freezing. *Microscopy and Microanalysis* **2008**, *14* (5), 375–379. https://doi.org/10.1017/S1431927608080781.

(7) Punjani, A.; Rubinstein, J. L.; Fleet, D. J.; Brubaker, M. A. CryoSPARC: Algorithms for Rapid Unsupervised Cryo-EM Structure Determination. *Nat Methods* **2017**, *14* (3), 290–296. https://doi.org/10.1038/nmeth.4169.

(8) Rubinstein, J. L.; Brubaker, M. A., Alignment of cryo-EM movies of individual particles by optimization of image translations. *Journal of Structural Biology* **2015,** *192* (2), 188-195. https://doi.org/10.1016/j.jsb.2015.08.007.

(9) Punjani, A.; Zhang, H.; Fleet, D. J. Non-Uniform Refinement: Adaptive Regularization Improves Single-Particle Cryo-EM Reconstruction. *Nature Methods* **2020**, *17* (12), 1214–1221. https://doi.org/10.1038/s41592-020-00990-8.

(10) Scheres, S. H. W. RELION: Implementation of a Bayesian Approach to Cryo-EM Structure Determination. *Journal of Structural Biology* **2012**, *180* (3), 519–530. https://doi.org/10.1016/j.jsb.2012.09.006.

(11) Zivanov, J.; Nakane, T.; Scheres, S. H. W. A Bayesian Approach to Beam-Induced Motion Correction in Cryo-EM Single-Particle Analysis. *IUCrJ* **2019**, *6*, 5–17. https://doi.org/10.1107/S205225251801463X.

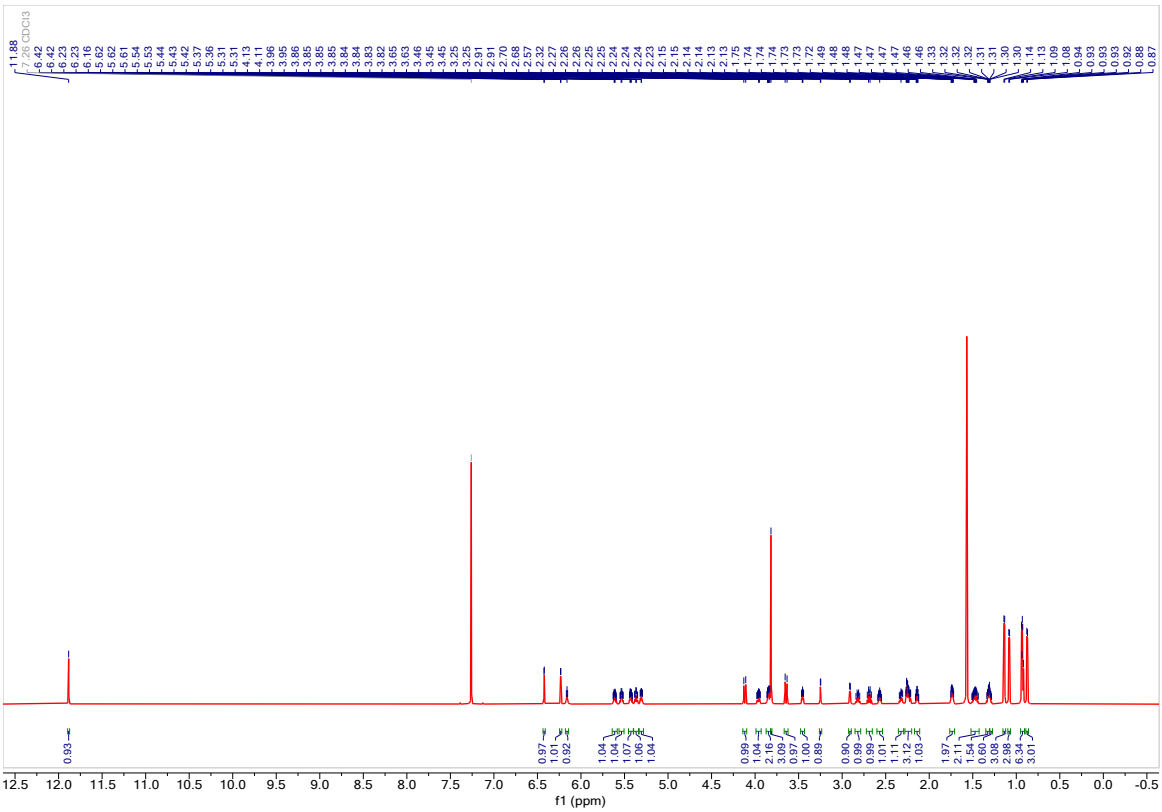

Figure S1: ^{1}H NMR Compound **2** (800 MHz, $CDCl_3$)

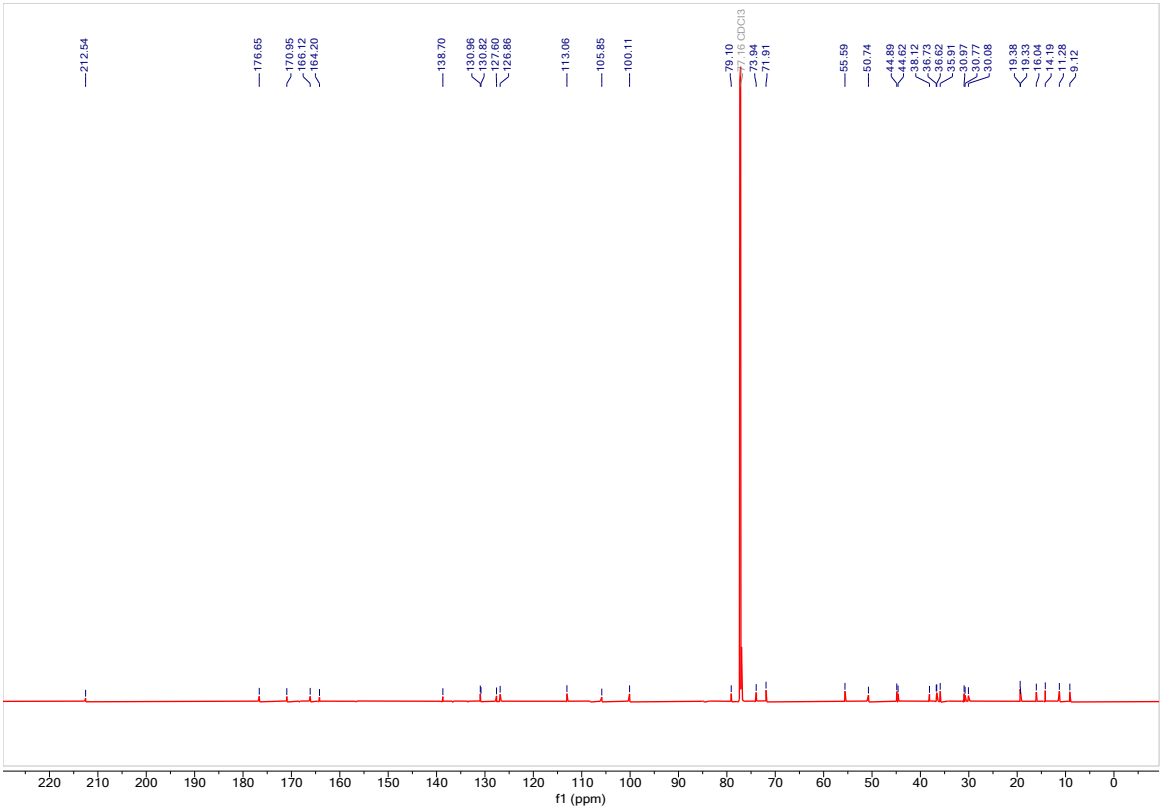

Figure S2: ^{13}C{1H} NMR Compound **2** (101 MHz, $CDCl_3$)

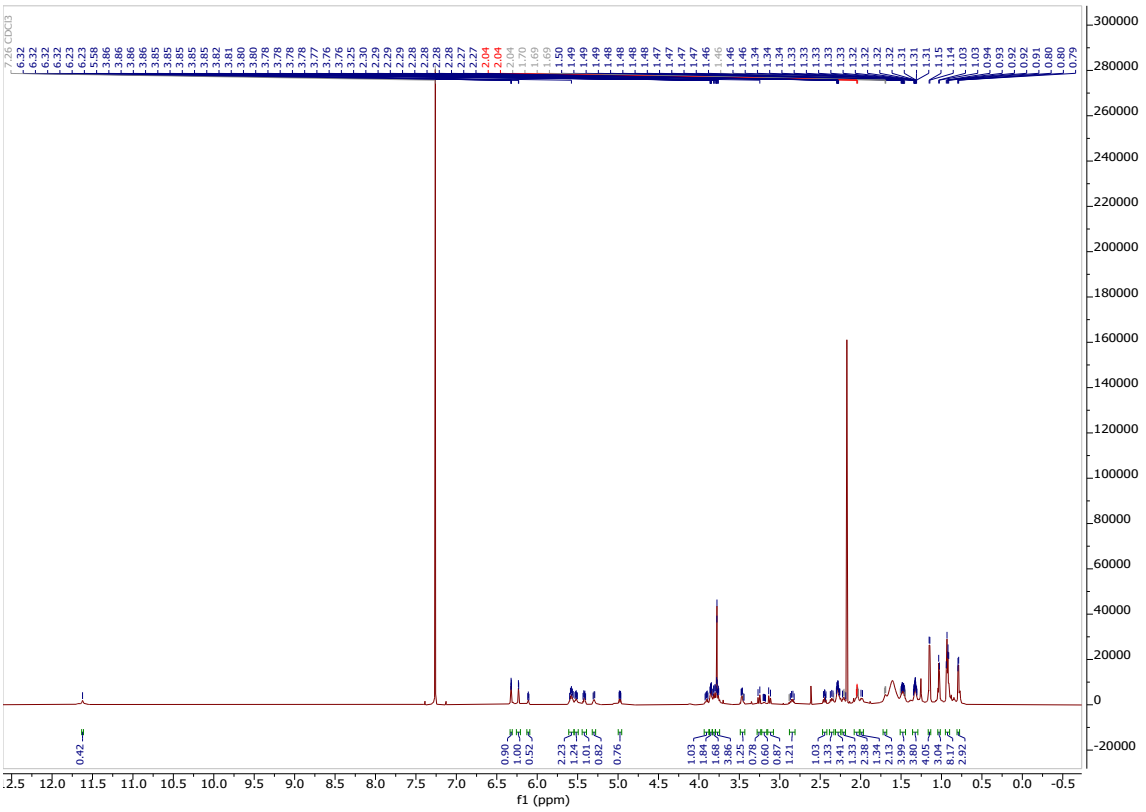

Figure S3: ^{1}H NMR Compound **3** (800 MHz, $CDCl_3$)

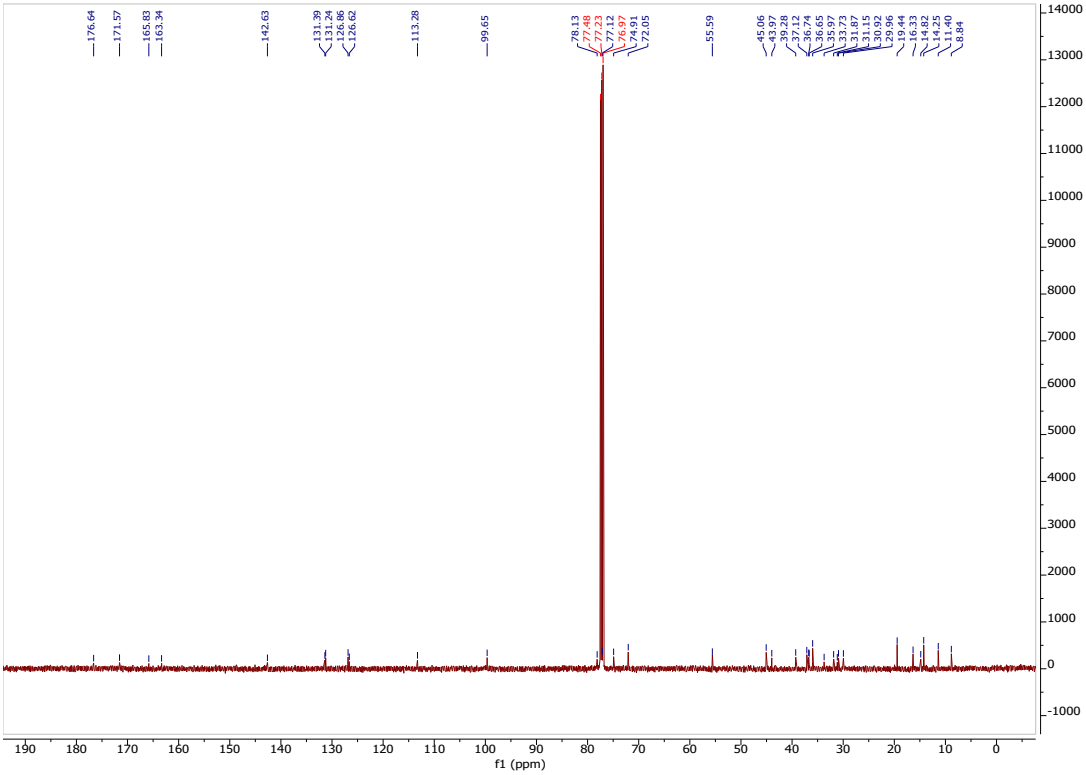

Figure S4: ^{13}C{1H} NMR Compound **3** (101 MHz, $CDCl_3$)

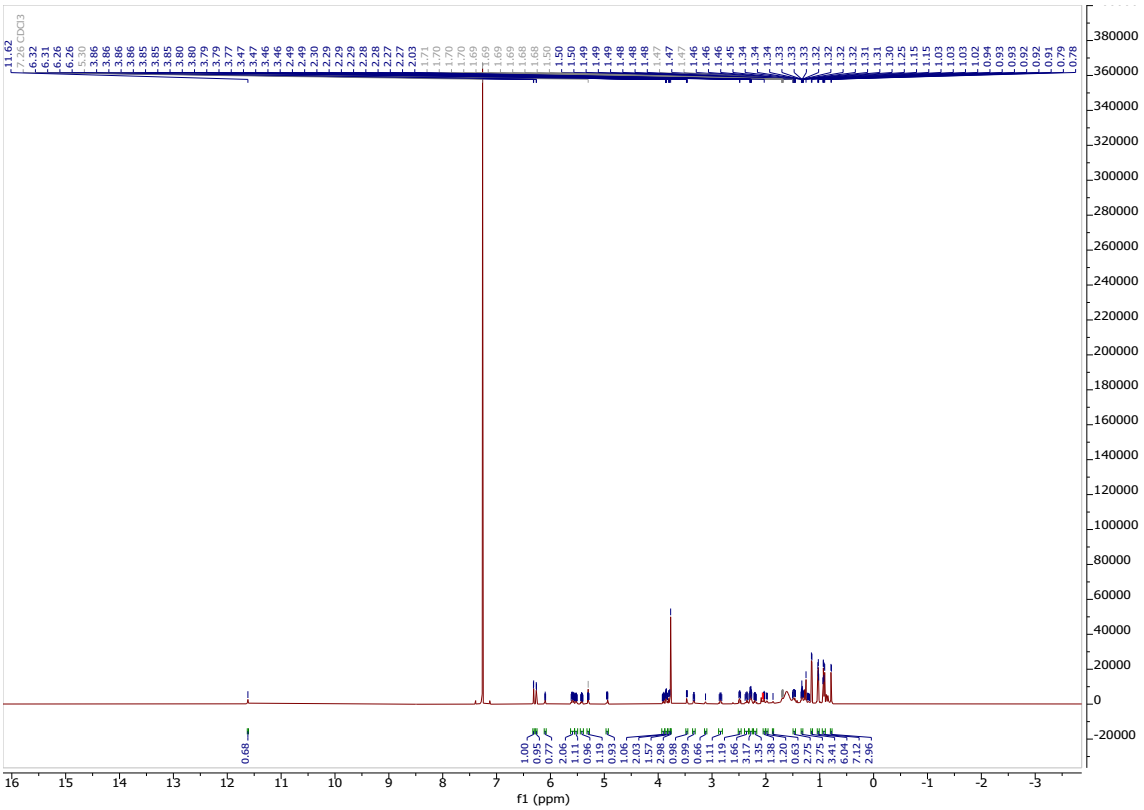

Figure S5: ^{1}H NMR compound **4** (800 MHz, $CDCl_3$)

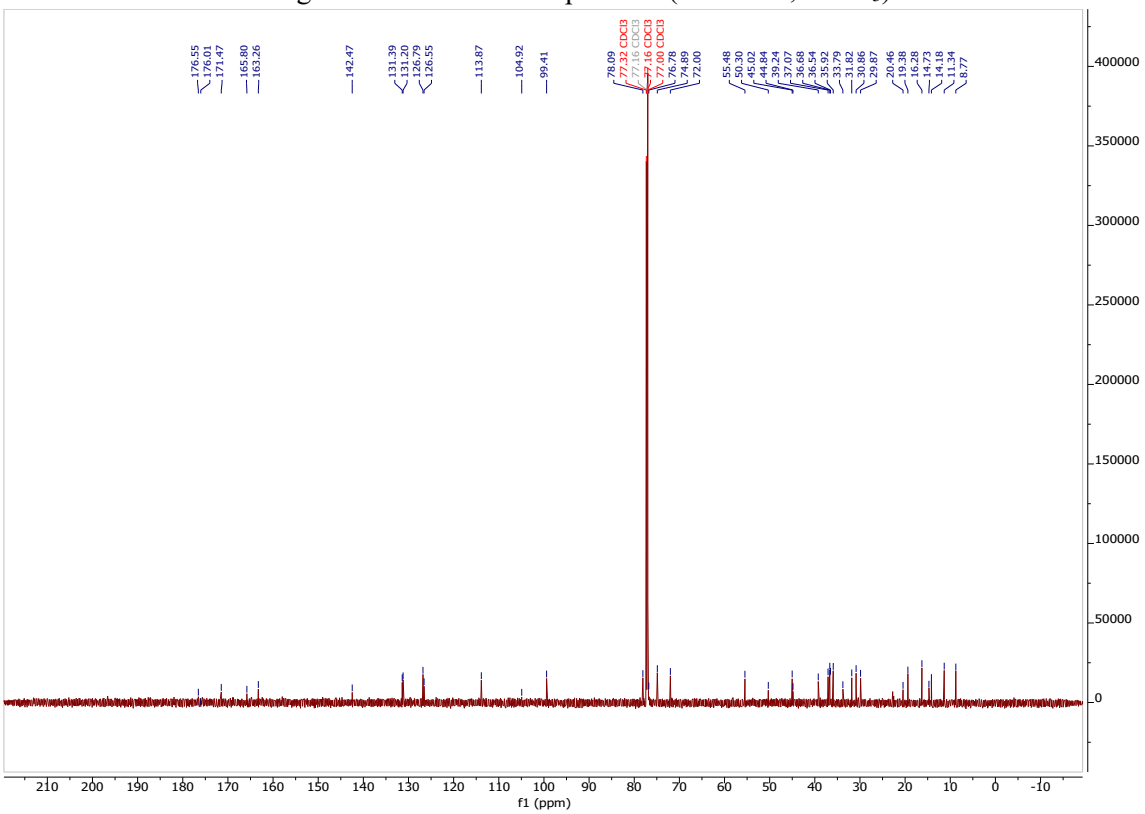

Figure S6: $^{13}C\{1H\}$ NMR compound **4** (101 MHz, $CDCl_3$)

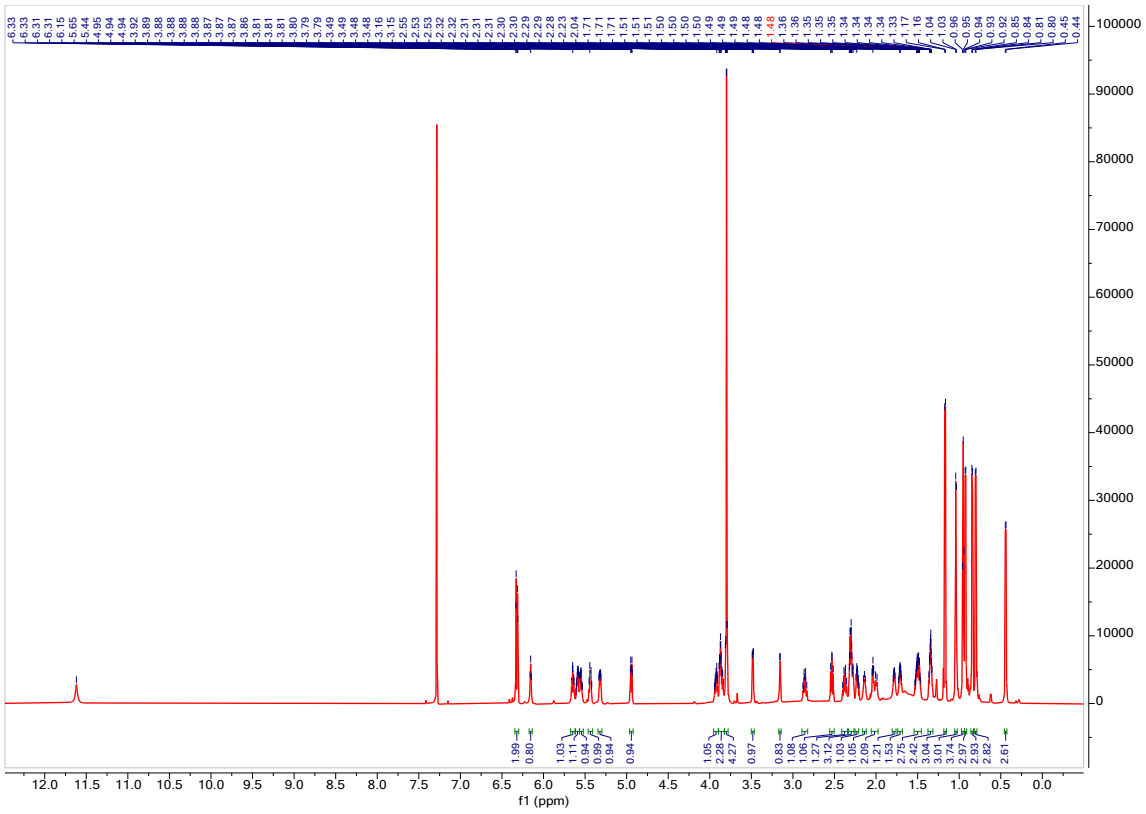

Figure S7: ^{1}H NMR compound **5** (800 MHz, $CDCl_3$)

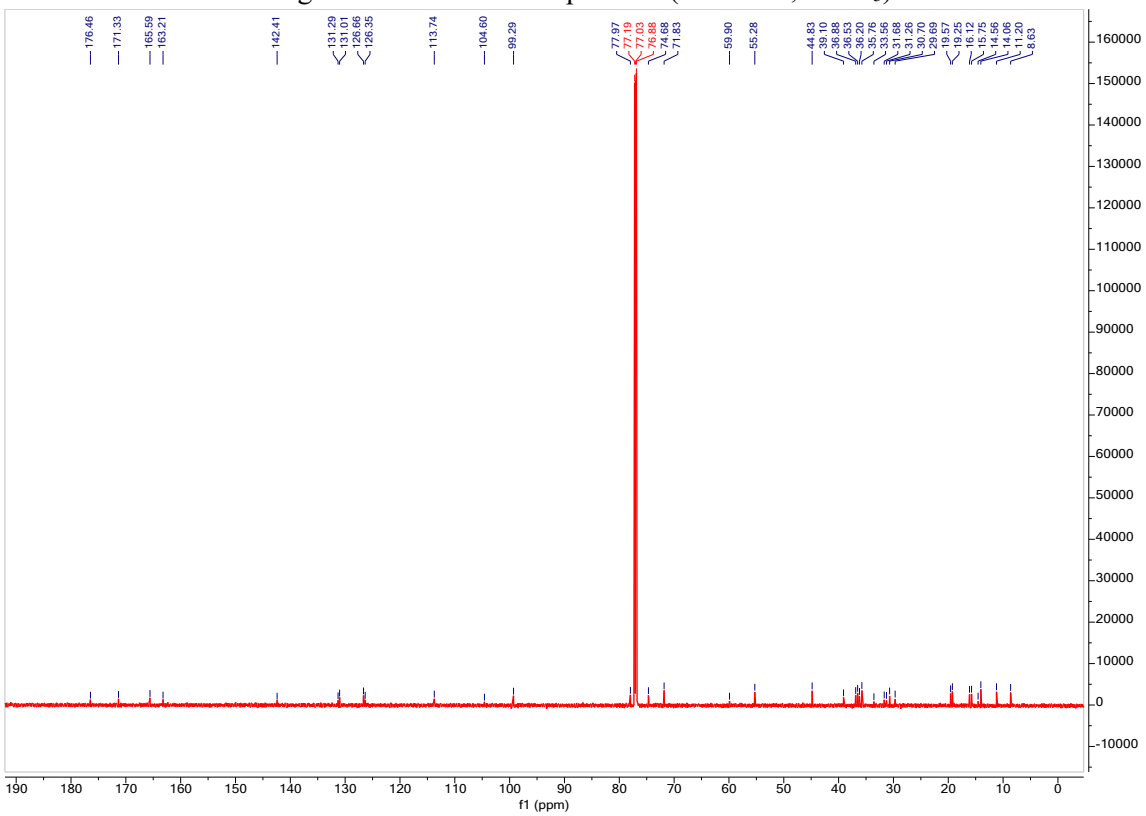

Figure S8: ^{13}C{1H} NMR compound **5** (101 MHz, $CDCl_3$)

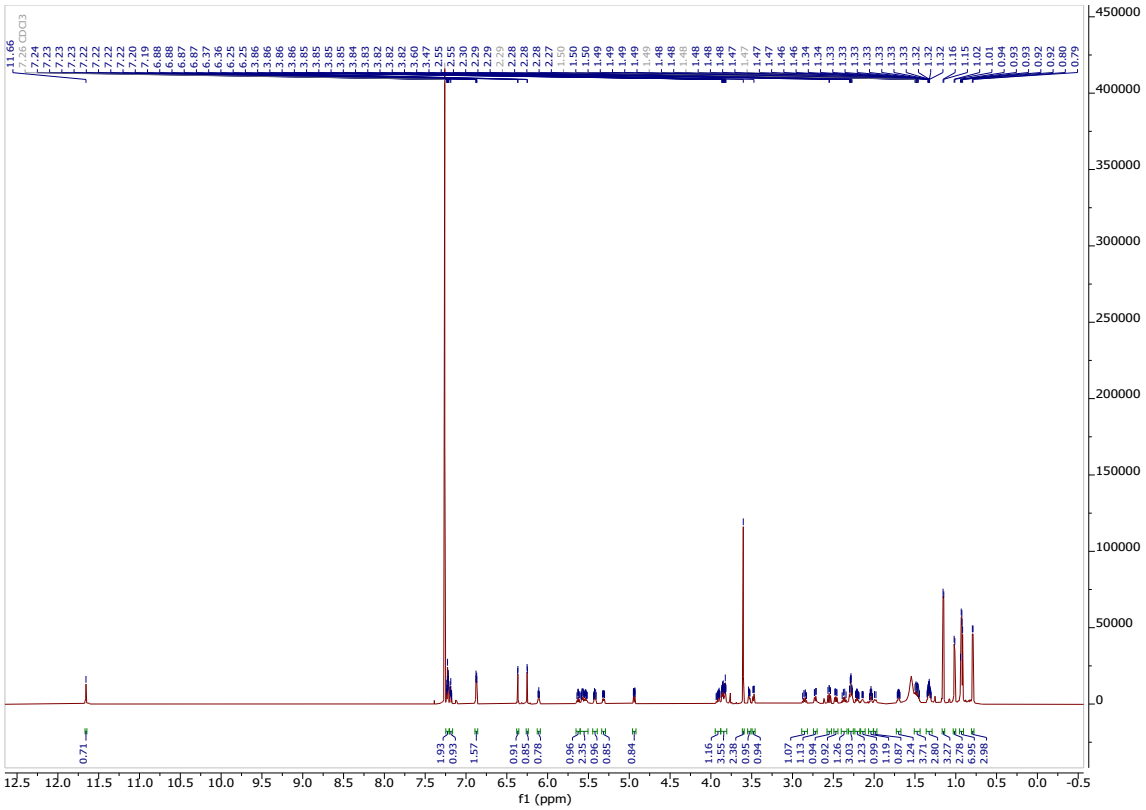

Figure S9: ^{1}H NMR compound **6** (800 MHz, $CDCl_3$)

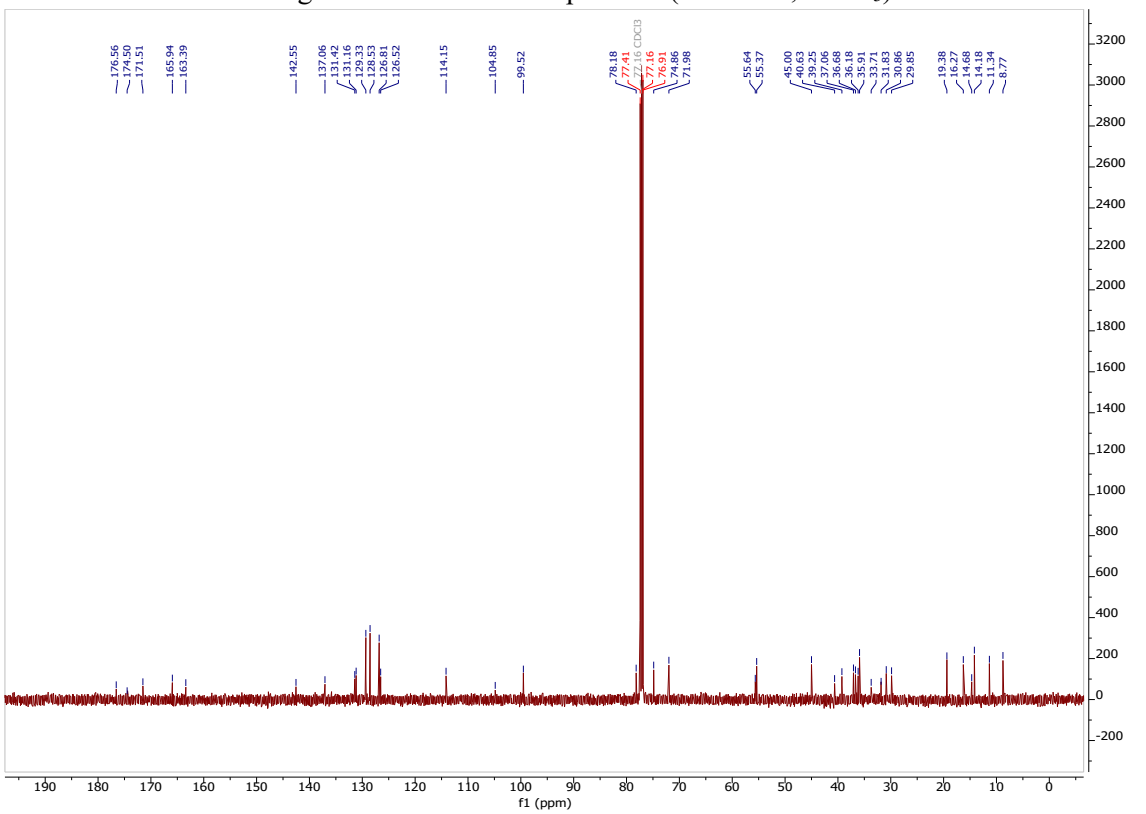

Figure S10: ^{13}C{1H} NMR compound **6** (101 MHz, $CDCl_3$)

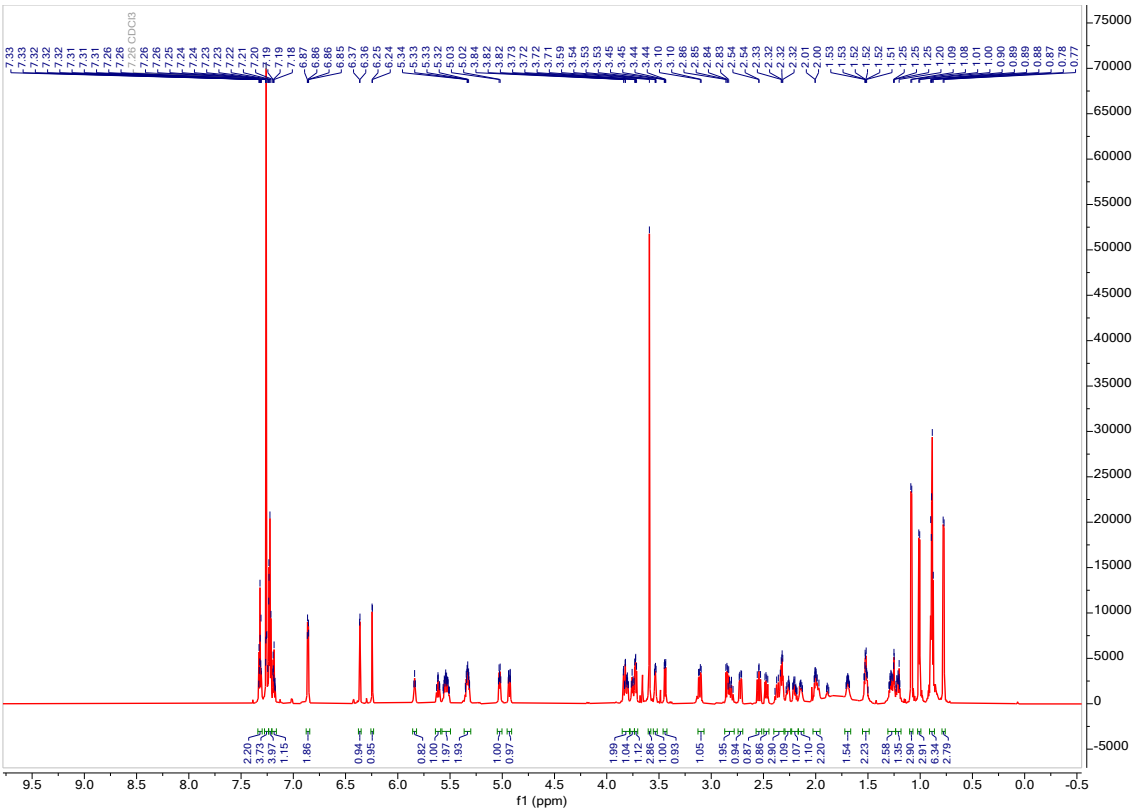

Figure S11: ^{1}H NMR compound **7** (800 MHz, $CDCl_3$)

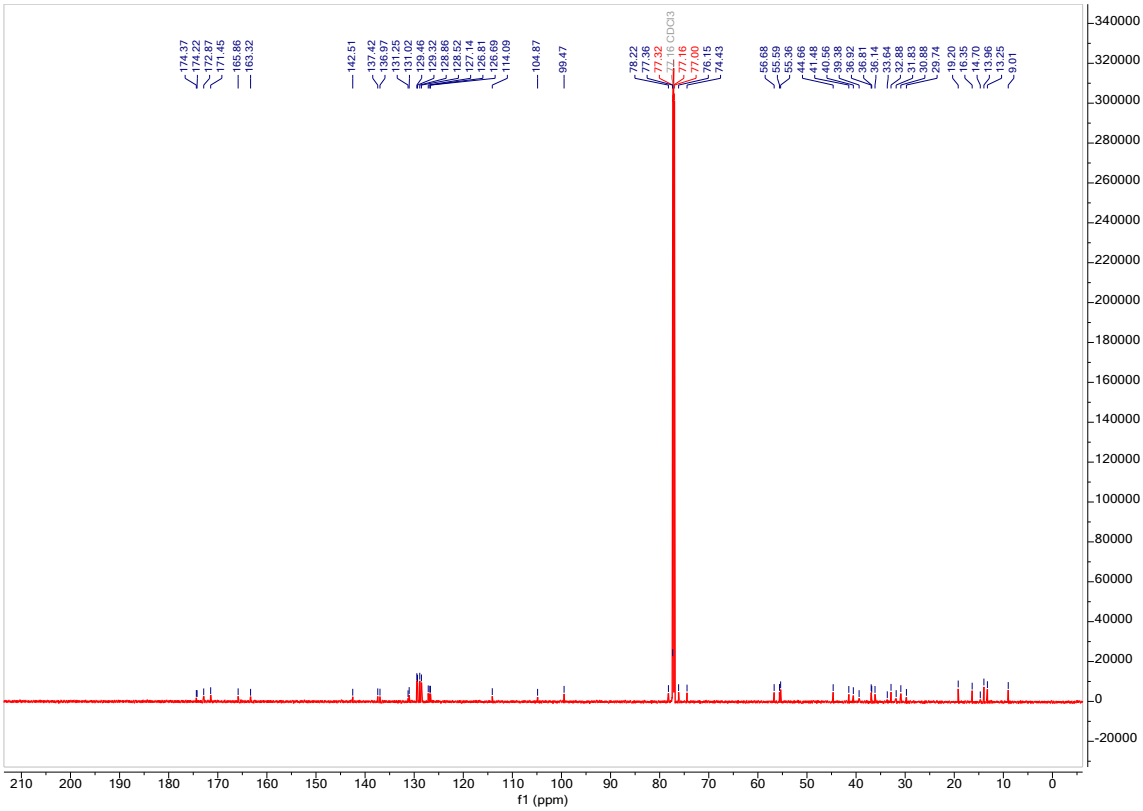

Figure S12: ^{13}C{1H} NMR compound **7** (101 MHz, $CDCl_3$)

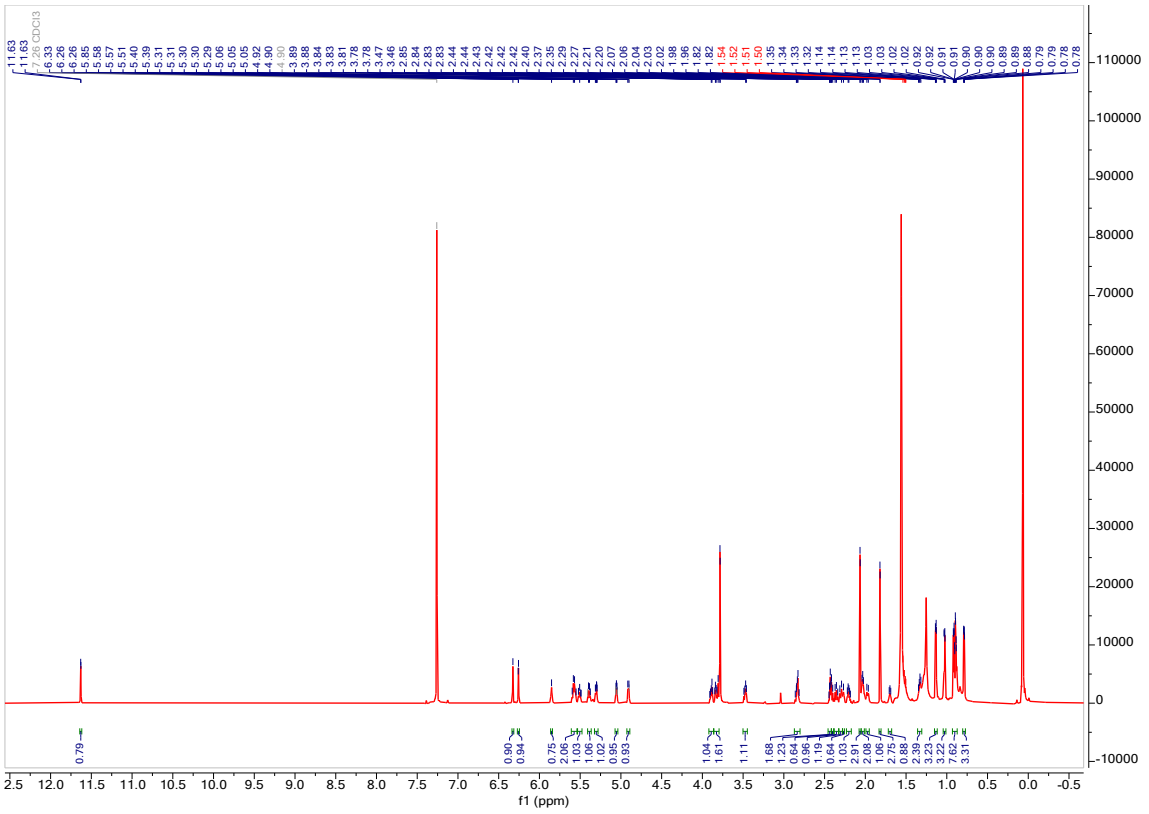

Figure S13: ^{1}H NMR compound **8** (800 MHz, $CDCl_3$)

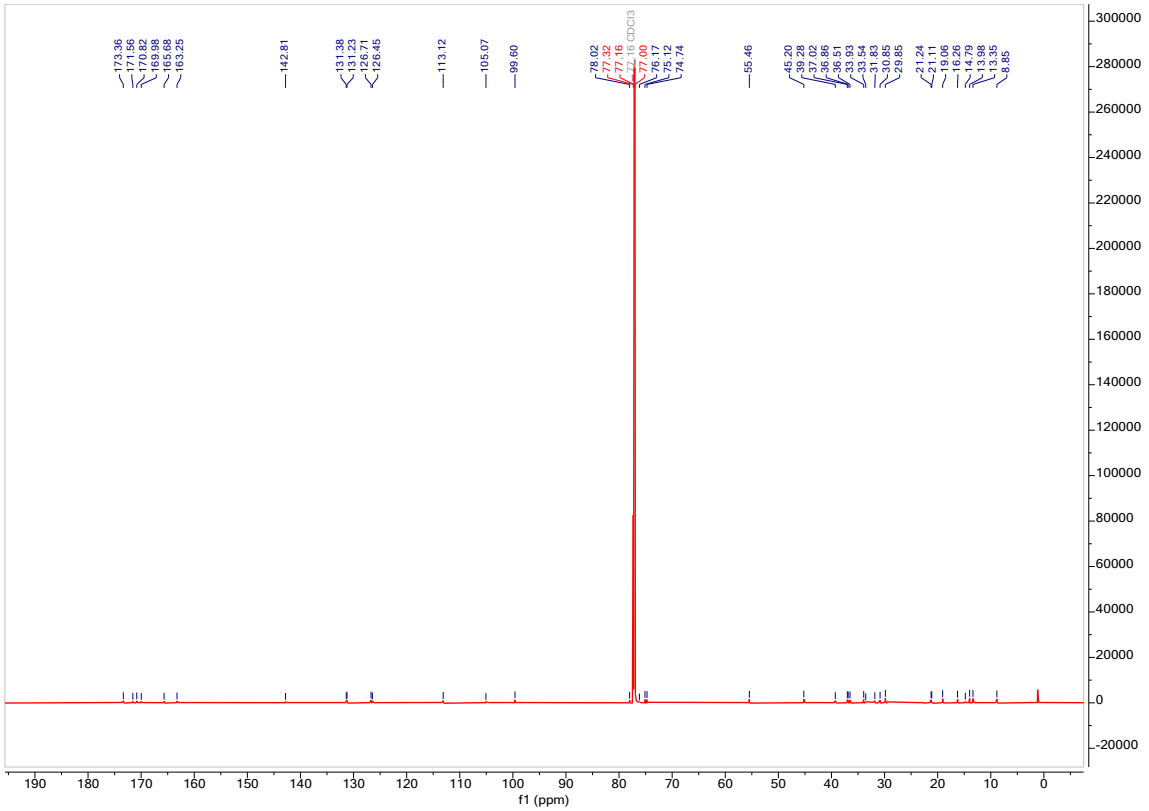

Figure S14: $^{13}C\{1H\}$ NMR compound **8** (101 MHz, $CDCl_3$)

Figure S15: ^{1}H NMR compound **9** (800 MHz, $CDCl_3$)

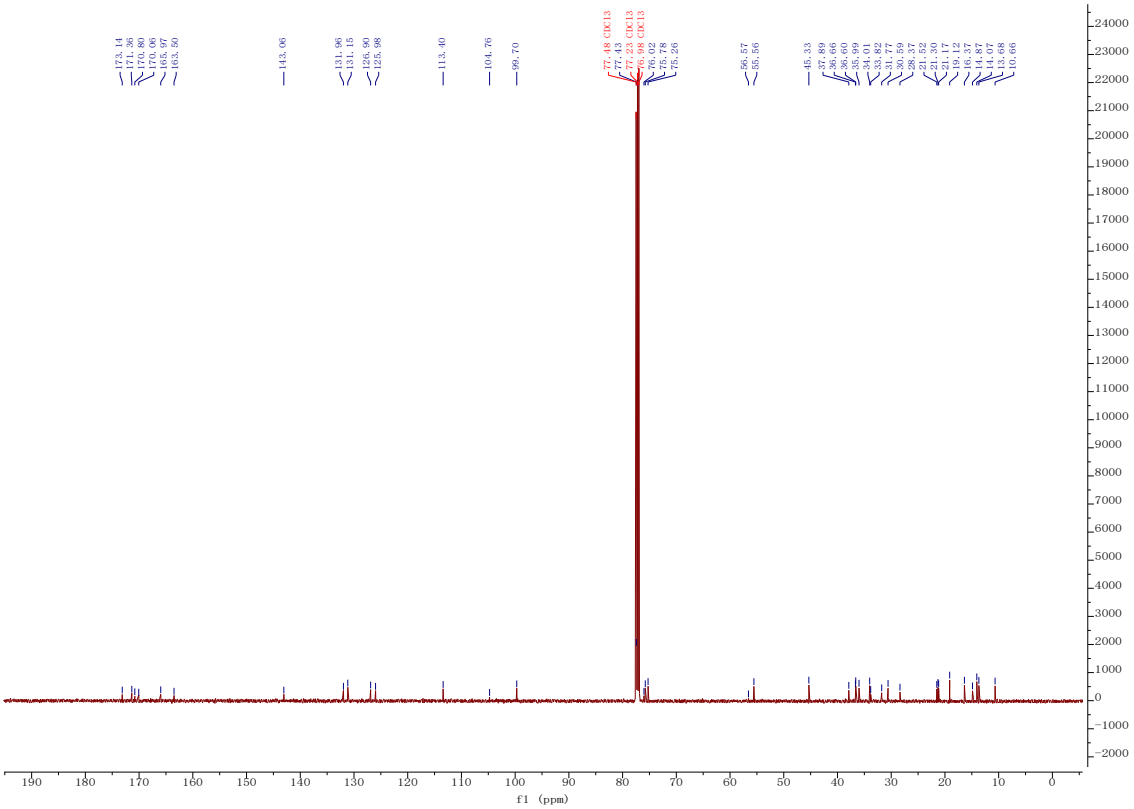

Figure S16: $^{13}C\{1H\}$ NMR compound **9** (101 MHz, $CDCl_3$)

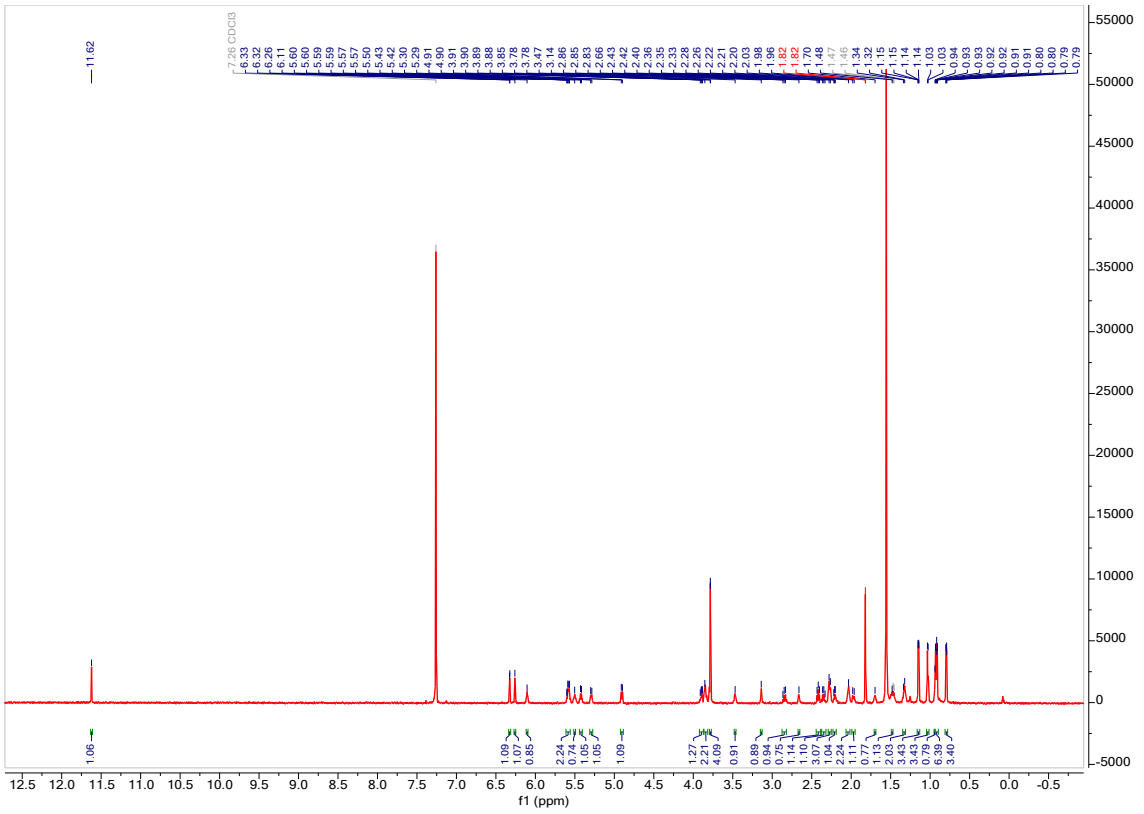

Figure S17: ^{1}H NMR compound **10** (800 MHz, $CDCl_3$)

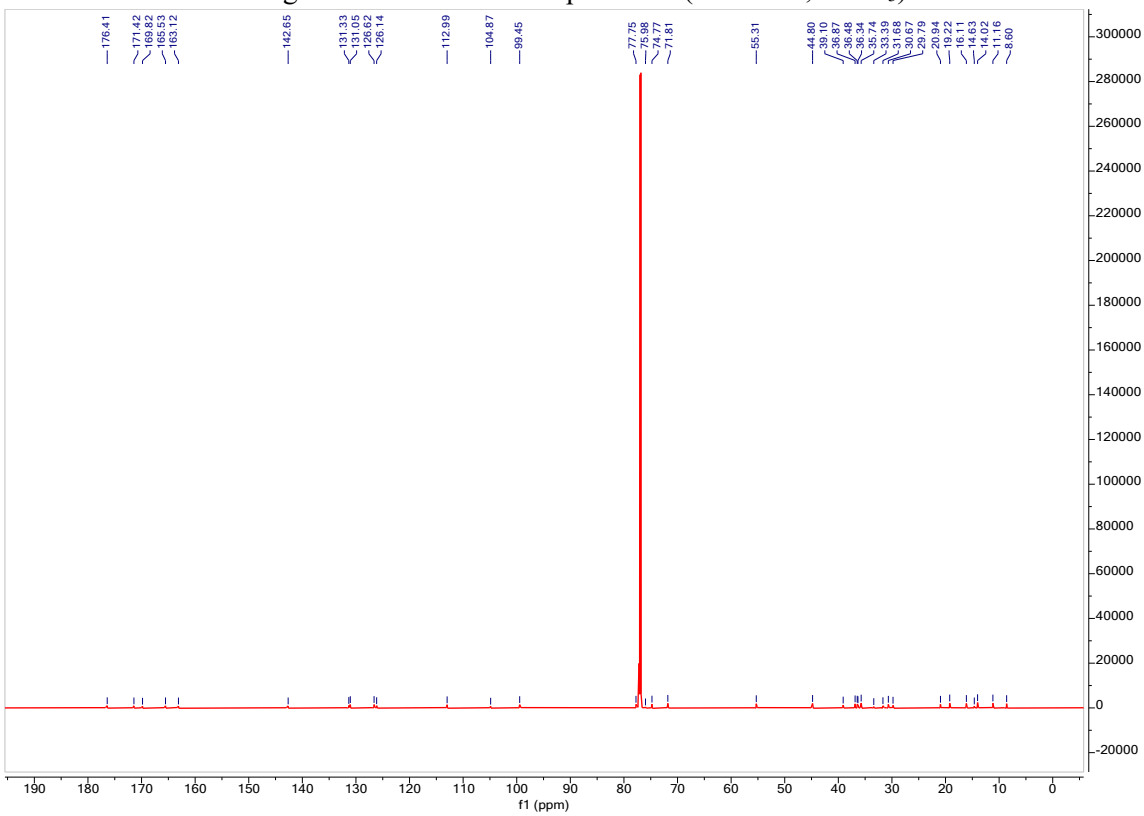

Figure S18: ^{13}C{1H} NMR compound **10** (101 MHz, $CDCl_3$)

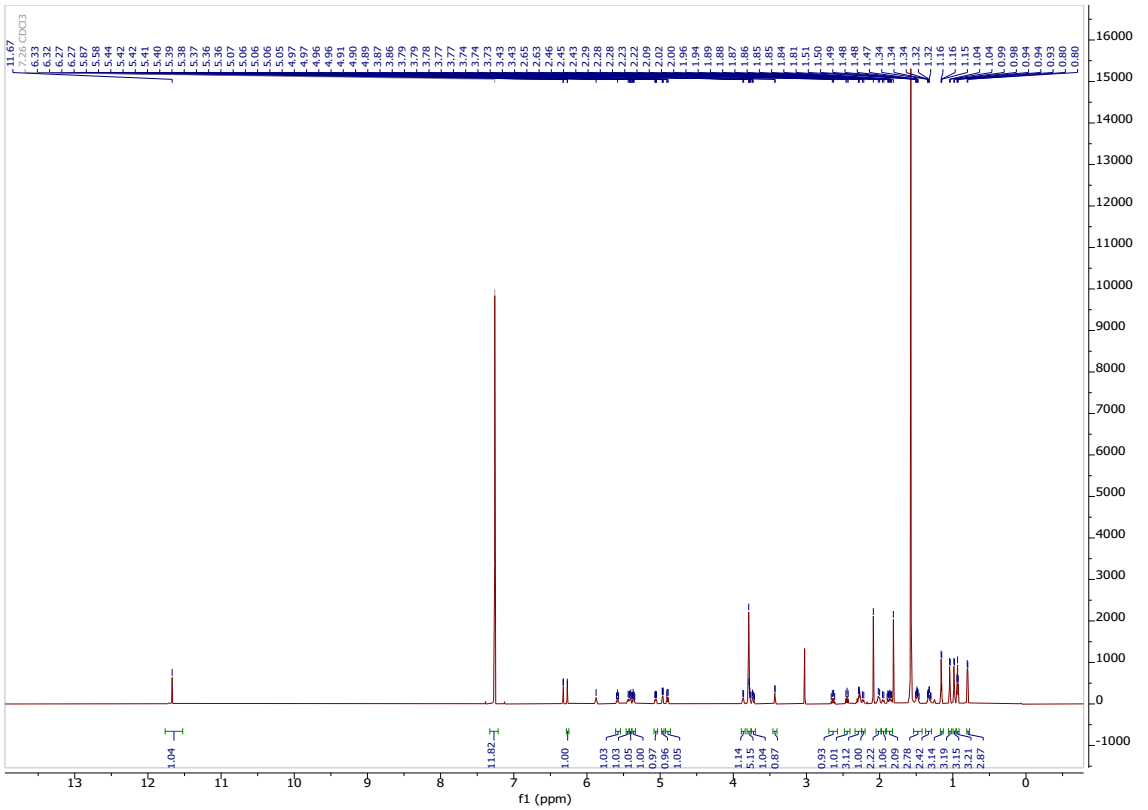

Figure S19: ^{1}H NMR compound **11** (800 MHz, $CDCl_3$)

Figure S20: ^{13}C{1H} NMR compound **11** (101 MHz, $CDCl_3$)

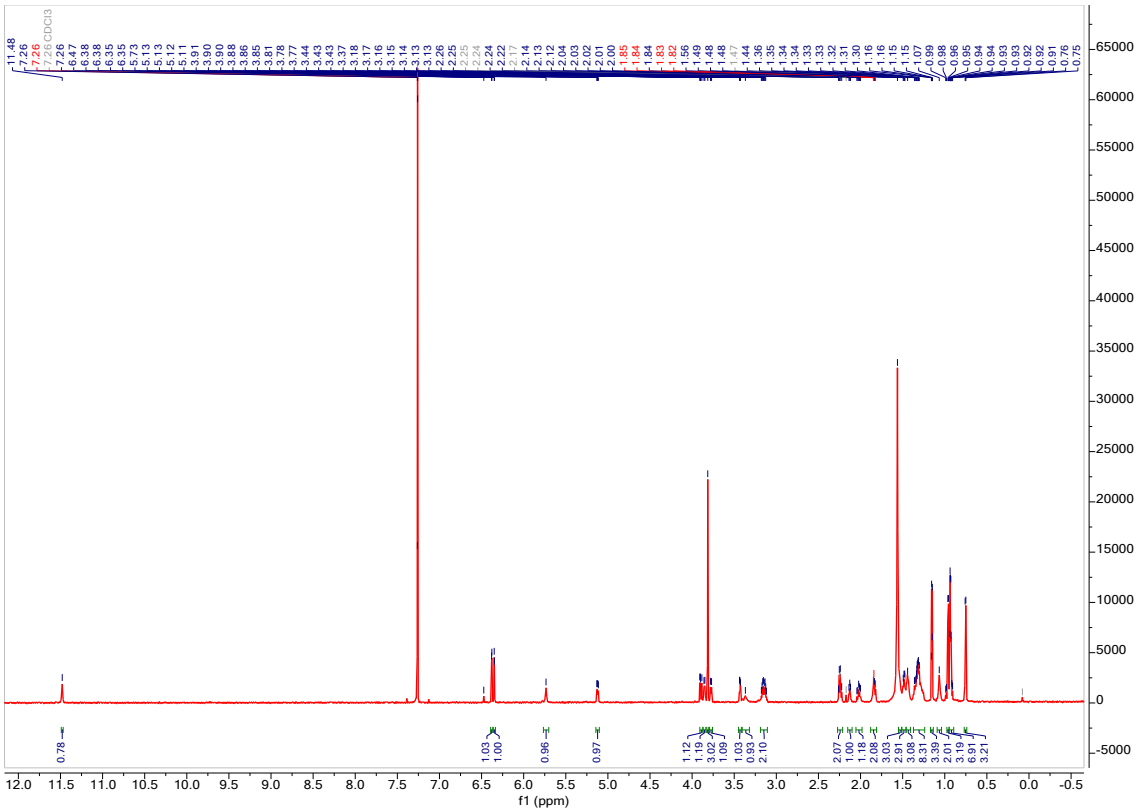

Figure S21: ^{1}H NMR compound **12** (800 MHz, $CDCl_3$)

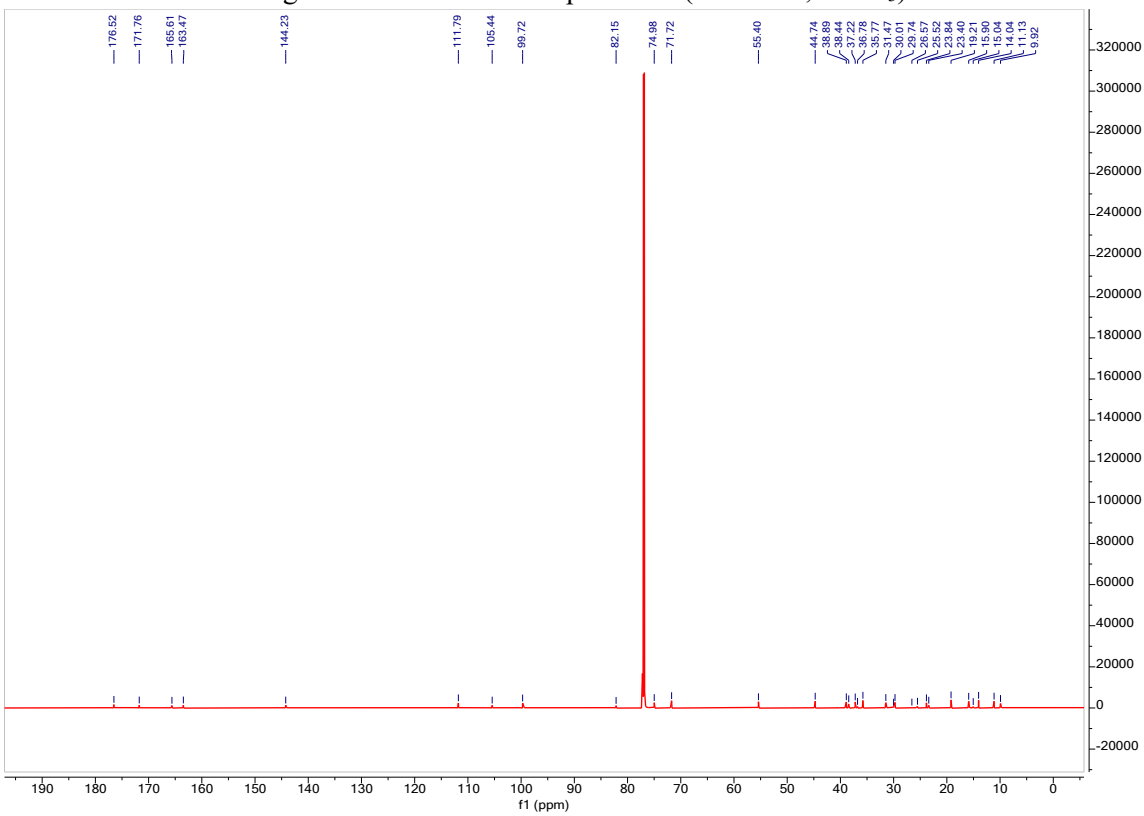

Figure S22: ^{13}C{1H} NMR compound **12** (101 MHz, $CDCl_3$)

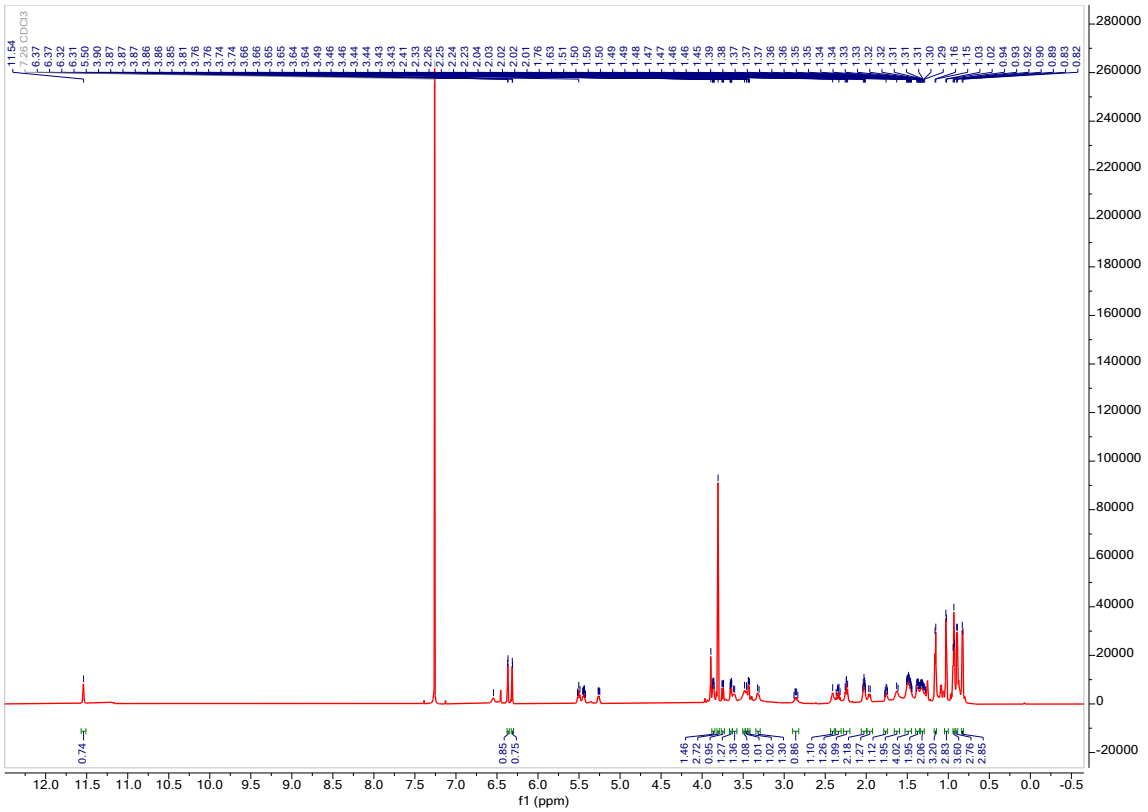

Figure S23: ^{1}H NMR compound **14** (800 MHz, $CDCl_3$)

Figure S24: ^{13}C{1H} NMR compound **14** (101 MHz, $CDCl_3$)

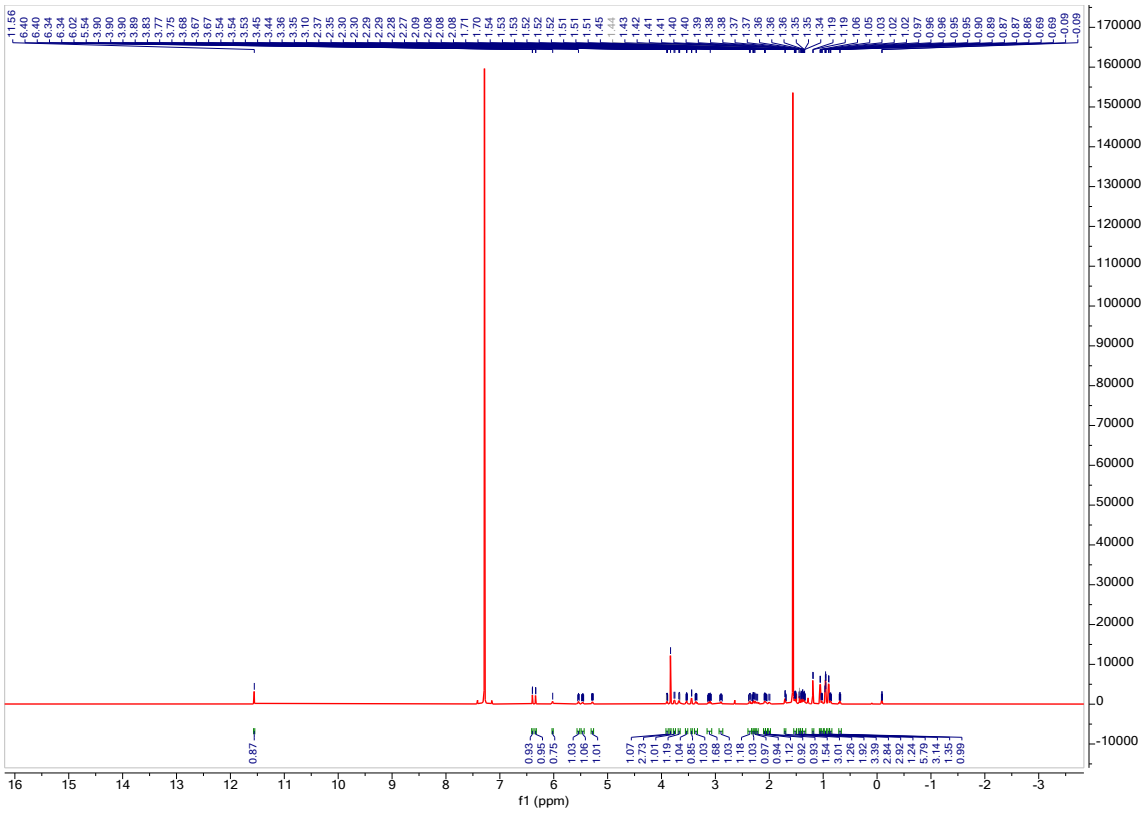

Figure S25: ^{1}H NMR compound **15** (800 MHz, $CDCl_3$)

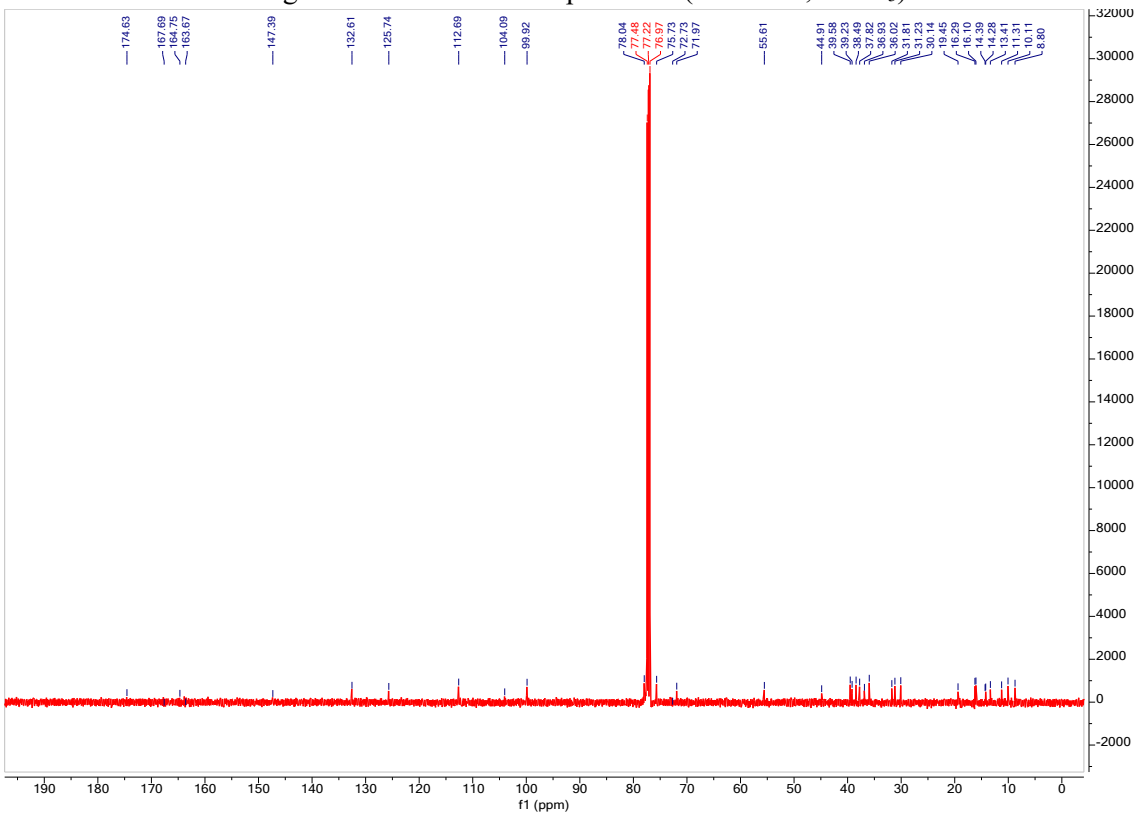

Figure S26: ^{13}C{1H} NMR compound **15** (101 MHz, $CDCl_3$)

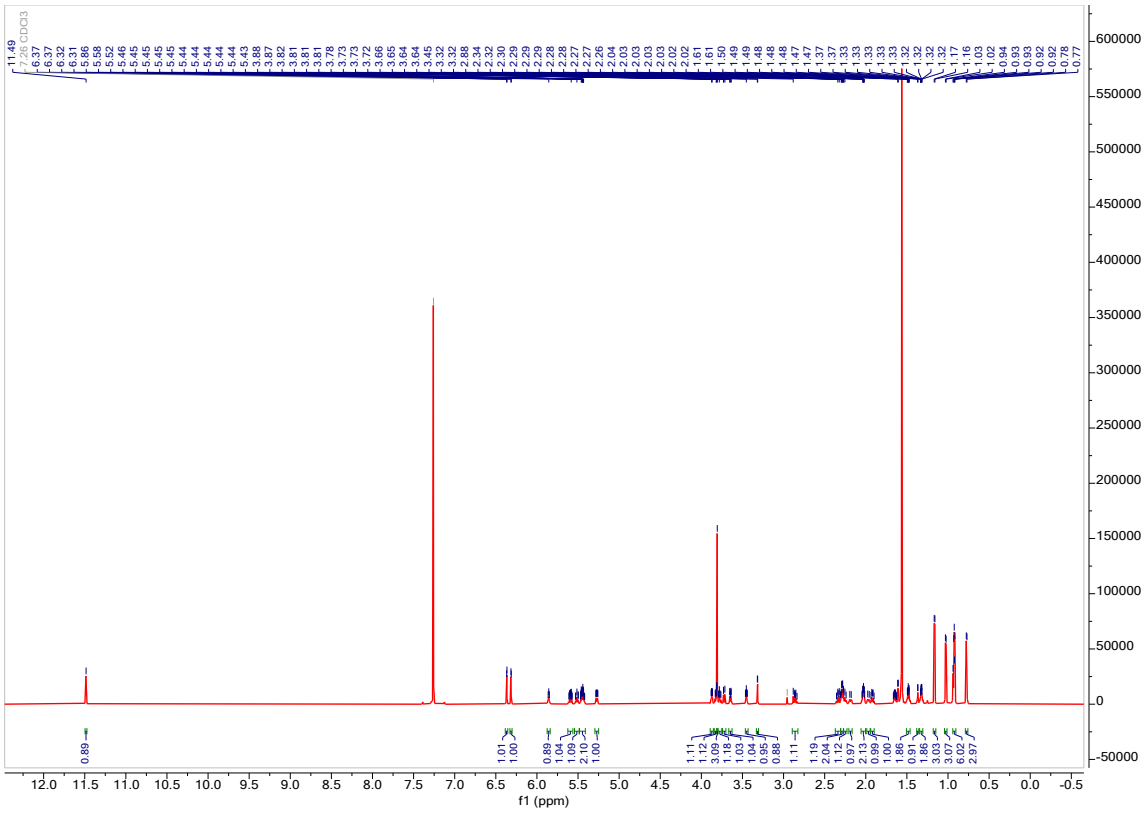

Figure S27: ^{1}H NMR compound **16** (800 MHz, $CDCl_3$)

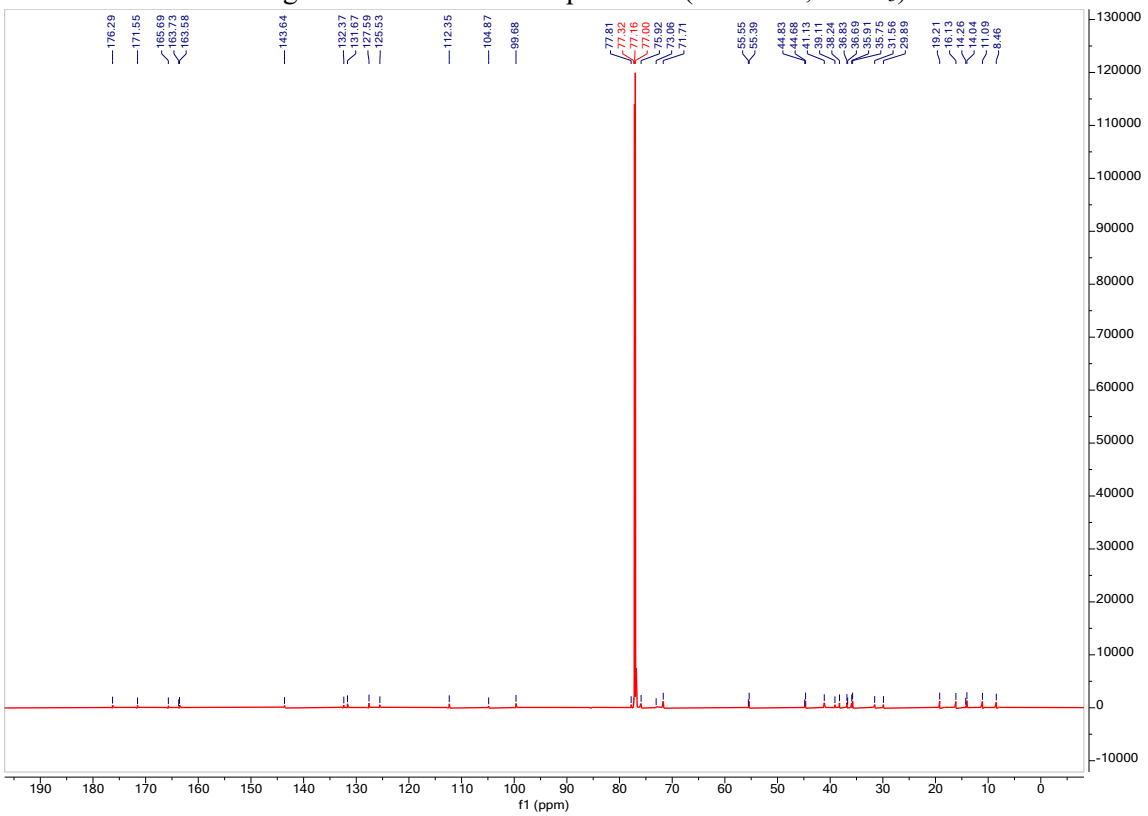

Figure S28: ^{13}C{1H} NMR compound **16** (101 MHz, $CDCl_3$)